Autoidentification Method of the “Trouble Maker(s)” for Internal Instability in Multiparalleled Inverters System

Wu, Weimin; Zhao, Zhijun; Koutroulis, Eftichis; Chung, Henry Shu-Hung; Blaabjerg, Frede

Published in:
IEEE Transactions on Industrial Electronics

DOI (link to publication from Publisher):
10.1109/TIE.2021.3053881

Publication date:
2022

Document Version
Accepted author manuscript, peer reviewed version

Auto-Identification Method of the "Trouble Maker(s)" for Internal Instability in Multi-paralleled Inverters System

Weimin Wu, *Member, IEEE*, Zhijun Zhao, Eftichis Koutroulis, *Senior Member*, *IEEE*, Henry Shu-Hung Chung, *Fellow*, *IEEE*, and Frede Blaabjerg, *Fellow, IEEE*

***Abstract*—The instability of power systems comprising multiple LCL-filtered grid-connected DC/AC inverters connected in parallel, can be caused by any individual inverter due to mutual coupling through the grid impedance. For the stability analysis of a multi-paralleled DC/AC inverters system, an effective technique capable to diagnose which particular inverter (i.e. "trouble maker") causes instability to the overall system has not yet been developed. In this paper, a novel auto-identification method is proposed to detect the "trouble maker(s)" of instability in a multi-paralleled inverters system, based on the comparison between the Root Mean Square (RMS) value of harmonic voltage at the point of common coupling (PCC) and the harmonic voltages across the filters capacitors. The theoretical analysis of the proposed identification method is presented in details in this paper. Also, simulation and experimental results are provided for verification of the effectiveness of the proposed technique.**

***Index Terms*--Grid-connected DC/AC inverter, Multi-paralleled inverters, Internal instability, Auto-identification method, LCL-filter.**

I. Introduction

With the rapid development of renewable energy sources, grid-connected DC/AC inverters have been researched widely as interfaces connecting the renewable energy sources to the electric grid [1]. The DC/AC inverters with an LCL-type output filter are considered as a preferred choice, due to better suppression of switching harmonics and lower cost [2]. However, the inherent resonance of LCL filters may cause instability to the overall system. Different damping methods have been studied to address this challenge, e.g. [3], [4]. The stability of an inverter system has been analyzed by an impedance-based approach in [5] and a state-space-based method in [6]. Utilizing these methods, many measures can be used to improve the system stability [7],[8].

However, even if an inverter is individually well designed and stable, when multiple inverters are connected in parallel to the electric grid, new problems may still appear. Especially, the interaction between the multi-paralleled inverters system and the electric grid may lead to resonance and even instability [8]-[11]. The interactive instability (i.e. instability caused by the interaction between the multi-paralleled inverters and the grid) often occurs under weak grid conditions. In [13], [14], and [15], the authors analyzed the interactive stability of DC/AC inverters systems by applying the impedance-based method. The interactive instability results from the interactions between the inner current or voltage control loops and the network passive components and the grid impedance. The interactive instability of multi-paralleled grid-connected inverters systems is closely related to the electric grid impedance and the number of paralleled inverters. However, this method has been established based on the precondition that each inverter system is internally stable under an ideal grid state condition.

Meanwhile, the internal stability of a multi-paralleled inverters system has also been studied extensively. Differently from the interactive instability, the internal instability may occur even under stiff grid conditions. It results from the DC/AC inverter parameters drift, improper design or internal errors. In [16], [17], and [18], the internal stability of multi-paralleled grid-connected inverters systems has been analyzed and it was concluded that the internal stability is only determined by the loop gain of the current control loop of the inverter, independently of the grid impedance and the number of paralleled inverters. This means that the internal instability of the inverter system may be caused by improper controller parameters, incorrect current sampling, and unreasonable filter design.

Different measures have been taken to improve the stability of multi-parallel inverter systems [18]-[21]. In [18], the LCL filter and control parameters were redesigned to meet the requirements of internal and interactive stability, while the active damper literature [19], [20] and improved notch filter [21] were used to solve the stability problem of multiple parallel inverters system.

In real industrial applications, it is important to exactly identify the inverter (named as "trouble maker") that causes instability [20], [23], [24], when the overall multi-paralleled grid-connected inverters system is unstable. The state-space-

Manuscript received August 7, 2020; revised November 3, 2020; revised December 13, 2020; accepted January 9, 2021. Date of publication; date of current version. This work was supported in part by the National Natural Science Foundation of China under Grant 51877130, in part by the National Key Research and Development Project of China under Grant 2017YFGH001164 and in part by the program "Bilateral and Multilateral Research & Technology Co-operation between Greece and China" under Grants 2017YFGH001164 and eSOLAR/T7ΔΚΙ-00066. Recommended for publication by Associate Editor *****. (Corresponding author: Weimin Wu.)

W. Wu and Z. Zhao are with the Electrical Engineering Department, Shanghai Maritime University, Shanghai 201306, China (e-mail: wmwu@shmtu.edu.cn; 201830210047@stu.shmtu.edu.cn).

E. Koutroulis is with the School of Electrical and Computer Engineering, Technical University of Crete, Chania 73100, Greece (e-mail: efkout@electronics.tuc.gr).

H. S.-H. Chung is with the Department of Electrical Engineering and the Centre for Smart Energy Conversion and Utilization Research, City University of Hong Kong, Hong Kong (e-mail: eeshc@cityu.edu.hk).

F. Blaabjerg is with the Energy Engineering Department, Aalborg University, Aalborg 9100, Denmark (e-mail: fbl@et.aau.dk).

based method can be used to tackle this problem through the participation factor (PF) by using the space-state matrix [20]. Nevertheless, this method is not appropriate in a large-scale power system with a large number of DC/AC converters connected, due to the complex formulation of the state matrices. Wang *et al.*[23] analyzed that the contribution of a given inverter on system stability can be determined by the ratio of inverter output admittance to the equivalent admittance of the rest of the system. Cao *et al.* in [24] proposed a method to determine the responsibility of each inverter on system harmonic instability quantitatively, based on global admittance. However, these two methods in [22] and [23] can be only used subject to the assumption that each inverter in the overall system is internally stable. Thus, when the overall multi-paralleled grid-connected inverters system is in internal instability conditions, it is important to apply a method for the identification of the particular "trouble maker(s)" DC/AC inverter(s). However, such an effective method is currently not available.

In order to fill this gap, in this paper, a simple and effective method is proposed to diagnose which inverter(s) is (are) the "trouble maker(s)", when internal instability has been developed in a multi-paralleled grid-connected inverters system. It is based on comparison between the RMS value of harmonic voltage at the point of common coupling (PCC) and the harmonic voltage across the filters capacitors when the internal instability occurs in the overall interconnected system.

The rest of this paper is organized as follows. The instability contribution analysis based on impedance methods is carried out in Section II. In Section III, the proposed method to automatically identify the "trouble maker(s)" of internal instability is introduced. Then, the simulation results based on the MATLAB/ Simulink platform, as well as the experimental results based on the control hardware of dSPACE DS1202 are presented in Section IV in order to verify the effectiveness of the proposed method. Finally, conclusions are drawn in Section V.

II. MODELING OF MULTI-PARALLELED GRID-CONNECTED INVERTERS SYSTEM

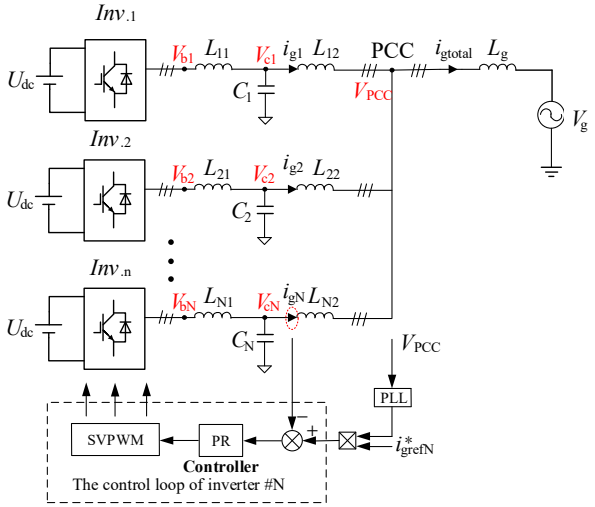

Fig.1. Topology of the multi-paralleled grid-connected inverters system.

Fig. 1 shows N paralleled inverters are connected to the electric grid at the PCC. V_{bi} is the output voltage of #i inverter. V_{ci} represents the capacitor voltage of the LCL-filter of the #i inverter. The voltage of PCC is represented as V_{PCC}. L_{i1}, L_{i2} and C_i(i=1, 2,…, N) represent the inverter-side inductor, grid-side inductor, and filter capacitor, respectively. L_g is the grid inductor. i_{gi}, i_{gtotal} represent the grid-injected current of Inverter #i and the total grid-injected current of the multi-paralleled grid-connected inverters system, respectively. In this paper, the PLL bandwidth is designed to be 14 Hz to ensure that the system does not have synchronization instability under weak grid conditions [25]. The current control structure of each DC/AC inverter is shown in Fig. 2. The grid-injected current i_g is controlled to track its reference i_{gref}. G_c(s) represents the transfer function of the current controller. The gain of the inverter, G_{inv}(s) is equal to 1, when the Space Vector Pulse Width Modulation (SVPWM) is used. G_d(s) is the delay time of the DC/AC inverter, which includes the computational delay and the modulation delay. Y_{f1}(s) and Y_{f2}(s) are the transfer functions of the LCL filter.

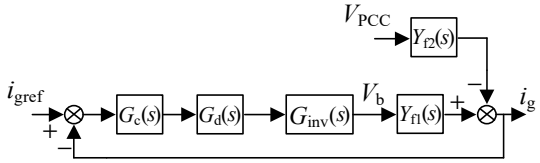

Fig.2. Current control block diagram of a grid-connected DC/AC inverter.

A PR controller in the stationary reference frame (the α-β frame) is chosen as current controller in this paper. The transfer function of the PR controller is described by

$$G_c(s) = K_P + \frac{K_r s}{s^2 + \omega_f^2} \tag{1}$$

where ω_f is the fundamental angular frequency, while K_P and K_r are the proportional gain and the resonant gain, respectively, of the PR controller.

The transfer function of the delay time of the DC/AC inverter is described by a third-order Pade approximation, which is written as:

$$G_d(s) = e^{-1.5T_s} \approx \frac{-(1.5T_s s)^3 + 12(1.5T_s s)^2 - 60(1.5T_s s) + 120}{(1.5T_s s)^3 + 12(1.5T_s s)^2 + 60(1.5T_s s) + 120} \tag{2}$$

where T_s is the sampling period.

Y_{f1}(s)and Y_{f2}(s) are the transfer functions from the grid-connected current i_g to the inverter output voltage V_b and from the grid-connected current i_g to the voltage of PCC, respectively. Y_{f1}(s) and Y_{f2}(s) are expressed as:

$$\begin{aligned} Y_{f1}(s) &= \frac{Z_C(s)}{Z_{11}(s)Z_C(s) + Z_{11}(s)Z_{12}(s) + Z_{12}(s)Z_C(s)} \\ Y_{f2}(s) &= \frac{Z_{11}(s) + Z_C(s)}{Z_{11}(s)Z_C(s) + Z_{11}(s)Z_{12}(s) + Z_{12}(s)Z_C(s)} \end{aligned} \tag{3}$$

Then, the grid-injected current can be derived as follows:

$$i_g(s) = \frac{T(s)}{1+T(s)} i_{gref}(s) - \frac{Y_{f2}(s)}{1+T(s)} V_{PCC}(s) \tag{4}$$

where T(s) is the open-loop gain of the current loop. T(s) is described as:

$$T(s)=G_{\mathrm{C}}(s)G_{\mathrm{d}}(s)G_{\mathrm{inv}}(s)Y_{\mathrm{f1}}(s) \tag{5}$$

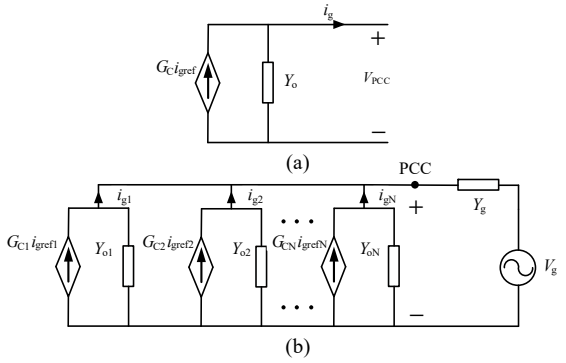

Fig.3. (a) Impedance model of a grid-connected DC/AC inverter, (b) impedance model of a multi-parallel grid-connected inverters system.

The current control block of the grid-injected current is equivalent to the Norton model, which is shown in Fig. 3(a). $G_{\mathrm{c}}i_{\mathrm{gref}}$ and Y_{o} are the controlled current source and equivalent output admittance of the inverter, respectively. They are given by:

$$G_{\mathrm{c}}i_{\mathrm{gref}}(s)=\frac{T(s)}{1+T(s)}i_{\mathrm{gref}}(s),\ \ Y_{\mathrm{o}}(s)=\frac{Y_{\mathrm{f2}}(s)}{1+T(s)} \tag{6}$$

Then, the Norton models of N-paralleled grid-connected inverters are presented in Fig. 3(b). Y_{o1}, Y_{o2},…, Y_{oN} are the inverter output admittances and Y_{g} is the grid admittance. The grid-injected currents of the individual inverters, i_{g1}, i_{g2},…, i_{gN} are deduced as:

$$\begin{bmatrix} i_{\mathrm{g1}} \\ i_{\mathrm{g2}} \\ \vdots \\ i_{\mathrm{gN}} \end{bmatrix}=\begin{bmatrix} \mathrm{G}11 & \mathrm{M}12 & \cdots & \mathrm{M}1N & R1 \\ \mathrm{M}21 & \mathrm{G}22 & \cdots & \mathrm{M}2N & R2 \\ \vdots & \vdots & \ddots & \vdots & \vdots \\ \mathrm{M}N1 & \mathrm{M}12 & \cdots & \mathrm{G}NN & R\mathrm{N} \end{bmatrix}\begin{bmatrix} G_{\mathrm{c1}}i_{\mathrm{gref1}} \\ G_{\mathrm{c2}}i_{\mathrm{gref2}} \\ \vdots \\ G_{\mathrm{cN}}i_{\mathrm{grefN}} \\ V_{\mathrm{g}} \end{bmatrix} \tag{7}$$

$$\begin{aligned} G_{\mathrm{ii}} &= 1-\frac{Y_{\mathrm{oi}}}{Y_{\mathrm{o1}}+Y_{\mathrm{o2}}+\cdots+Y_{\mathrm{oN}}+Y_{\mathrm{g}}} \\ M_{\mathrm{i,j}} &= -\frac{Y_{\mathrm{oi}}}{Y_{\mathrm{o1}}+Y_{\mathrm{o2}}+\cdots+Y_{\mathrm{oN}}+Y_{\mathrm{g}}}(i\neq j) \\ R_{\mathrm{i}} &= \frac{Y_{\mathrm{oi}}\cdot Y_{\mathrm{g}}}{Y_{\mathrm{o1}}+Y_{\mathrm{o2}}+\cdots+Y_{\mathrm{oN}}+Y_{\mathrm{g}}} \end{aligned} \tag{8}$$

where G_{ii} and $M_{\mathrm{i,j}}$ represent the influence of the $G_{\mathrm{ci}}i_{\mathrm{grefi}}$ of the #i inverter and of the$G_{\mathrm{cj}}i_{\mathrm{grefj}}$ of the #j inverter, respectively, on the value of i_{gi}, respectively. The influence of the electric grid on i_{gi} is described by R_{i}.

The same denominator polynomials appear in (8). Thus, the stability of the grid-injected currents of the individual inverters, i_{g1},i_{g2},…, i_{gN}, are determined by the roots of the denominator polynomial in (8). Furthermore, with the polynomial in (8) divided by Y_{g}, a common polynomial (9) can be derived:

$$S_{\mathrm{i}}=\frac{Y_{\mathrm{oi}}}{1+T_{\mathrm{m}}},\ T_{\mathrm{m}}=\frac{Y_{\mathrm{o1}}+Y_{\mathrm{o2}}+\cdots+Y_{\mathrm{oN}}}{Y_{\mathrm{g}}} \tag{9}$$

It is assumed that each controlled current source $G_{\mathrm{ci}}i_{\mathrm{grefi}}$ is stable and the output admittances of the individual inverters do not include poles in the right half-plane. Then, the stability of the grid-injected current of each individual inverter also depends on T_{m}. When T_{m} satisfies the Nyquist stability criterion, then the grid-injected current is stable, otherwise it is unstable.

Since the non-diagonal elements of (7) are not zero, the multi-paralleled grid-connected inverters are always coupled [10]. The coupling between the DC/AC inverters becomes stronger, as the grid impedance increases. Thus, the instability in a multi-paralleled inverters system finally results in that each of the grid-injected currents of the inverters and the voltage at the PCC are oscillating. From the waveforms of output voltage and current, it is difficult to identify which inverter (or inverters) causes the instability in the overall interconnected system.

III. Proposed Method to Automatically Identify the Unstable Inverter within a Multi-paralleled Inverters System

When oscillations and instabilities have been developed in a multi-paralleled DC/AC inverters system, each inverter of the system will not be providing power to the PCC. This may lead to an energy deficit in the electric grid and the inability to supply power to the grid consumers. Thus, a method for the automatic identification of the unstable inverter is useful and meaningful.

According to Fig. 1, assuming that Inverter #i operates under internal instability conditions, then an unstable control signal will cause an unstable voltage V_{bi}, which further causes oscillation in the capacitor voltage V_{ci} and in the voltage of the PCC through the LCL-filter, since the following equations apply:

$$\begin{aligned} V_{\mathrm{bi}} &= sL_{\mathrm{i1}}i_{\mathrm{Li1}}+V_{\mathrm{ci}}, \\ V_{\mathrm{PCC}} &= V_{\mathrm{ci}}-sL_{\mathrm{i2}}i_{\mathrm{gi}} \end{aligned} \tag{10}$$

Thus, as a source of oscillation and instability, Inverter #i delivers the unstable currents to the grid and other inverters, causing instability of the entire multi-paralleled grid-connected inverters system.

When the system is in steady state, the voltage of inductor L_{i2} is significantly lower than V_{PCC} and then V_{ci} can be viewed as almost equal to V_{PCC}. If Inverter #i causes system internal instability, then more high order harmonic currents of i_{gi}will exist in the grid inductor L_{i2}, causing more higher order harmonic voltages across inductor L_{i2}, which can be derived as

$$V_{\mathrm{PCCh}}=V_{\mathrm{cih}}-sL_{\mathrm{i2}}i_{\mathrm{gih}} \tag{11}$$

where V_{PCCh} and V_{cih} are the root mean square (RMS) values of high order harmonic voltages in V_{PCC} and V_{ci}, respectively, not including the fundamental component and dominant lower harmonics. According to [13]-[14], when the switching frequency of the DC/AC inverters is 10 kHz, then the unstable resonances of the multi-paralleled inverter system caused by the internal current control loop, exhibits a frequency that is up to several kHz. Thus, the high order harmonic current passing through the grid-side inductor L_{i2} comprises an important indication for the internal instability of the system.

When the system is in instability, the voltage of inductor L_{i2} is much higher than the voltage in stability and then V_{ci} is not equal to V_{PCC}.Thus, if any DC/AC inverter is operating under

internal instability conditions in a large multi-paralleled inverters system, it can be diagnosed as a "trouble maker" inverter from the overall inverters system by comparing the values of V_{ch} and V_{PCCh} developed in each individual inverter. In the following of this paper, the relationship between V_{ch} and V_{PCCh} is analyzed in details, when the system includes a single inverter (A) and N-paralleled inverters (B), respectively. Based on the analysis of (A) and (B), five steps used to automatically detect the "trouble maker(s)" DC/AC inverter(s) are proposed.

A. Comparison between V_{ch} and V_{PCCh} in a Single Inverter System

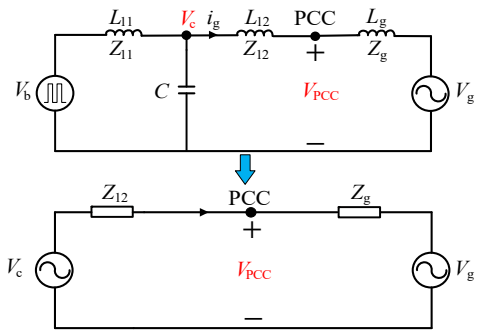

Fig.4 Simplified model of inverter when analyzing the relationship between V_{ch} and V_{PCCh}.

When comparing the capacitor voltage V_c and the voltage at PCC, a simplified model of the DC/AC inverter shown in Fig. 4 is used for further analysis. Pure inductance is chosen as grid impedance. A single-phase grid-connected inverter system is used to derive the relationship between V_{PCC} and V_c, which is also extended to a three-phase inverter system. The relationship between V_{PCC} and V_c is written as:

$$\begin{aligned} V_c &= Z_{12} i_g + V_{PCC} \\ V_c &= (Z_{12} + Z_g) i_g + V_g \end{aligned} \tag{12}$$

Further simplified, the relationship between V_{PCC} and V_c is rewritten as:

$$\begin{aligned} \frac{V_{PCC}}{V_c} &= 1 - (1 - \frac{V_g}{V_c}) \frac{Z_{12}}{Z_{12} + Z_g} \\ \frac{V_{PCCh}}{V_{ch}} &= 1 - (1 - \frac{V_{gh}}{V_{ch}}) \frac{Z_{12}}{Z_{12} + Z_g} \end{aligned} \tag{13}$$

When the multi-paralleled grid-connected inverter system is in instability, V_{PCCh} and V_{ch}, which are the parts of high frequency harmonics of V_{PCC} and V_c, are much higher than their corresponding values in the stable state. Moreover, the grid voltage V_g is pure and doesn't include high frequency harmonics. Then, the grid voltage at high frequency, V_{gh} is equal to 0. Therefore, equation (13) is rewritten as:

$$\frac{V_{PCCh}}{V_{ch}} = 1 - \frac{Z_{12}}{Z_{12} + Z_g} = 1 - \frac{L_{12}}{L_{12} + L_g} < 1 \tag{14}$$

Equation (14) indicates that the oscillating high frequency voltage is attenuated from V_c to V_{PCC}, when the DC/AC inverter is under the internal instability condition. Otherwise, V_{PCCh} is closer to V_{ch} as L_g improving is increased to higher values.

B. Comparison between V_{chi} (i=1,2,…,N) and V_{PCCh} in the Paralleled Grid-connected Inverters System

When analyzing the relationship between V_{cih} (i=1,2,…,N) and V_{PCCh}, the N-paralleled grid-connected inverters system is equivalent to the model presented Fig. 5. The N-paralleled inverters have identical parameters of LCL output filter.

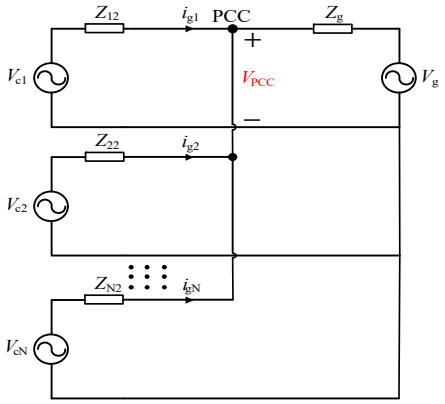

Fig. 5. Simplified model of an N-paralleled grid-connected inverters system when analyzing the relationship between V_{chi} (i=1, 2, …, N) and V_{PCCh}.

According to Fig. 5, the relationship between the filter capacitor voltages, the grid currents and voltage at PCC can be derived as:

$$\begin{aligned} V_{c1} &= Z_{12} i_{g1} + V_{PCC} \\ V_{c2} &= Z_{22} i_{g2} + V_{PCC} \\ &\cdots \\ V_{cN} &= Z_{N2} i_{gN} + V_{PCC} \end{aligned} \tag{15}$$

$$\begin{bmatrix} i_{g1} \\ i_{g2} \\ \cdots \\ i_{gN} \end{bmatrix} = \begin{bmatrix} G_{11} & G_{12} & \cdots & G_{1N} & G_{1(N+1)} \\ G_{21} & G_{22} & \cdots & G_{2N} & G_{2(N+1)} \\ \cdots & \cdots & \cdots & \cdots & \cdots \\ G_{N1} & G_{N2} & \cdots & G_{NN} & G_{N(N+1)} \end{bmatrix} \begin{bmatrix} V_{c1} \\ V_{c2} \\ \cdots \\ V_{cN} \\ V_g \end{bmatrix} \tag{16}$$

where

$$\begin{aligned} G_{11} &= \frac{1}{Z_{12} + Z_{22} \| \cdots \| Z_{N2} \| Z_g} \\ G_{12} &= \frac{1}{Z_{22} + Z_{12} \| Z_{32} \| \cdots \| Z_{N2} \| Z_g} \frac{Z_{32} + \cdots + Z_{N2} + Z_g}{Z_{12} + Z_{32} + \cdots + Z_{N2} + Z_g} \\ G_{1N} &= \frac{1}{Z_{N2} + Z_{12} \| Z_{22} \| \cdots \| Z_{(N-1)2} \| Z_g} \frac{Z_{22} + \cdots + Z_{(N-1)2} + Z_g}{Z_{12} + Z_{22} + \cdots + Z_{(N-1)2} + Z_g} \\ G_{1(N+1)} &= \frac{1}{Z_g + Z_{12} \| Z_{22} \| \cdots \| Z_{N2}} \frac{Z_{22} + \cdots + Z_{N2}}{Z_{12} + Z_{22} + \cdots + Z_{N2}} \end{aligned} \tag{17}$$

In (17), the symbol "||" represents the parallel combination of impedances. Since $G_{11}=G_{21}=\ldots=G_{N1}$, $G_{12} = G_{22} =\ldots= G_{N2}$, …, $G_{1N} = G_{2N} = \ldots = G_{NN}$, $G_{1(N+1)} = G_{2(N+1)} = \ldots = G_{N(N+1)}$, the ratio of V_{PCC} to V_{c1} can be derived as (18) and the ratio of V_{PCCh} and V_{c1h} can be derived as (19):

$$\begin{aligned} \frac{V_{PCC}}{V_{c1}} = 1 + (& \frac{1}{1 + \frac{Z_{22}}{Z_{12} \| Z_{32} \| \cdots \| Z_{N2} \| Z_g}} \frac{V_{c2}}{V_{c1}} + \cdots + \frac{1}{1 + \frac{Z_{N2}}{Z_{12} \| Z_{22} \| \cdots \| Z_{(N-1)2} \| Z_g}} \frac{V_{cN}}{V_{c1}} \\ & + \frac{1}{1 + \frac{Z_g}{Z_{12} \| Z_{22} \| \cdots \| Z_{N2}}} \frac{V_g}{V_{c1}} - \frac{1}{1 + \frac{Z_{22} \| Z_{32} \| \cdots \| Z_{N2} \| Z_g}{Z_{12}}}) \end{aligned} \tag{18}$$

$$\frac{V_{\mathrm{PCCh}}}{V_{\mathrm{c1h}}}=1+\left(\frac{1}{1+\dfrac{Z_{22}}{Z_{12}\|Z_{32}\|\cdots\|Z_{\mathrm{N2}}\|Z_{\mathrm{g}}}}\frac{V_{\mathrm{c2h}}}{V_{\mathrm{c1h}}}+\cdots+\frac{1}{1+\dfrac{Z_{\mathrm{N2}}}{Z_{12}\|Z_{22}\|\cdots\|Z_{(\mathrm{N-1})2}\|Z_{\mathrm{g}}}}\frac{V_{\mathrm{cNh}}}{V_{\mathrm{c1h}}}\right.$$
$$\left.+\frac{1}{1+\dfrac{Z_{\mathrm{g}}}{Z_{12}\|Z_{22}\|\cdots\|Z_{\mathrm{N2}}}}\frac{V_{\mathrm{gh}}}{V_{\mathrm{c1h}}}-\frac{1}{1+\dfrac{Z_{22}\|Z_{32}\|\cdots\|Z_{\mathrm{N2}}\|Z_{\mathrm{g}}}{Z_{12}}}\right) \tag{19}$$

Similarly, when the N-paralleled grid-connected inverters system is in stability, very small high frequency harmonics are developed in V_{c1},V_{c2},…, V_{cN} and V_{PCC}. Then, the values of V_{c1},V_{c2},…, V_{cN} at the fundamental frequency can be regarded as equal to V_{g}. Utilizing an identical equation shown in (20) and combining (18), the ratio of V_{c1} to V_{PCC} is equal to 1.

$$\frac{1}{1+\dfrac{Z_{22}}{Z_{12}\|Z_{32}\|\cdots\|Z_{\mathrm{N2}}\|Z_{\mathrm{g}}}}+\cdots+\frac{1}{1+\dfrac{Z_{\mathrm{N2}}}{Z_{12}\|Z_{22}\|\cdots\|Z_{(\mathrm{N-1})2}\|Z_{\mathrm{g}}}}$$
$$+\frac{1}{1+\dfrac{Z_{\mathrm{g}}}{Z_{12}\|Z_{22}\|Z_{32}\|\cdots\|Z_{\mathrm{N2}}}}-\frac{1}{1+\dfrac{Z_{22}\|Z_{32}\|\cdots\|Z_{\mathrm{N2}}\|Z_{\mathrm{g}}}{Z_{12}}}=0 \tag{20}$$

Therefore, the values of V_{PCC} and V_{c1} are equal when the system of N-paralleled grid-connected inverters is in stability.

When the N-paralleled grid-connected inverters system is in instability, it is assumed that Inverter #1 is internal instability and the rest Inverters #i (i=2, 3,… , N) are under internal stable operating conditions. Since Inverter #1 is internal instability, then it holds that $V_{\mathrm{c1h}}>V_{\mathrm{c2h}},\ldots,V_{\mathrm{c1h}}>V_{\mathrm{cNh}}$. As assumed above, V_{gh} is equal to 0. Therefore, together with (19) and (20), the ratio of V_{c1h} to V_{PCCh} can be derived as follows:

$$\frac{V_{\mathrm{PCCh}}}{V_{\mathrm{c1h}}}<1 \tag{21}.$$

Equation (21) indicates that the oscillating high frequency voltage is attenuated from V_{c1} to V_{PCC}, when Inverter #1 is in internal instability.

C. The Proposed Method to Automatically Identify the "Trouble Maker(s)" within the Inverters System

Five steps are used in the proposed method to detect the "trouble maker(s)" of instability in the multi-paralleled inverters system, when internal instability occurs. For the analyzed cases in this paper, the grid voltage is set equal to 110V. The flowchart of the proposed diagnosis process is shown in Fig. 6.

Step1: Calculate the values of V_{cih} and V_{PCCh}. According to the IEEE Std 519-2014, if the rated PCC voltage is below 1 kV, the total harmonic distortion (THD) of the PCC voltage should be within 8%. This paper chooses the THD value of V_{PCC} greater at 8% as the unstable condition. Thus, if V_{cih}< 8.8 V,V_{PCCh}< 8.8 V, then the multi-paralleled inverters system is stable and the process ends. Otherwise, the multi-paralleled inverters system is unstable and the diagnosis process continues to Step 2 described next, in order to detect the "trouble maker" inverter(s).

Step2: Calculate the values of V_{cih}-V_{PCCh}, and record the Inverter #k with the maximum value of V_{cih}-V_{PCCh}. According to (21), the Inverter #k is generally found from the inverters with the value of V_{cih}-V_{PCCh} higher than 0.

Step 3: Disconnect Inverter #k from the multi-paralleled inverters system and operate only the remaining system. Recalculate the values of V_{cih},V_{PCCh}.

Step 4: Investigate whether V_{cih}< 8.8 V,V_{PCCh}< 8.8 V is met. If these conditions are not satisfied, then the remaining system is still unstable and the proposed diagnosis process returns to Step 2 in order to calculate V_{cih}-V_{PCCh} again and disable the operation of Inverter #k until the overall system becomes stable.

Step 5: If V_{cih}< 8.8 V,V_{PCCh}< 8.8 V, then this implies that the multi-paralleled inverters system is stable. All disabled Inverters #k are recorded and they constitute the set of "trouble makers" in the multi-paralleled inverters system.

IV. Simulation and Experimental Verification

In order to verify the effectiveness of the proposed method, four 3kW/3-phase/110V paralleled inverters were modeled for simulations in the MATLAB/Simulink platform, where the parameters of system are listed in Table I. Also, three paralleled DC/AC inverter prototypes of 2.4kW/3-phase/110V were constructed for experiments.

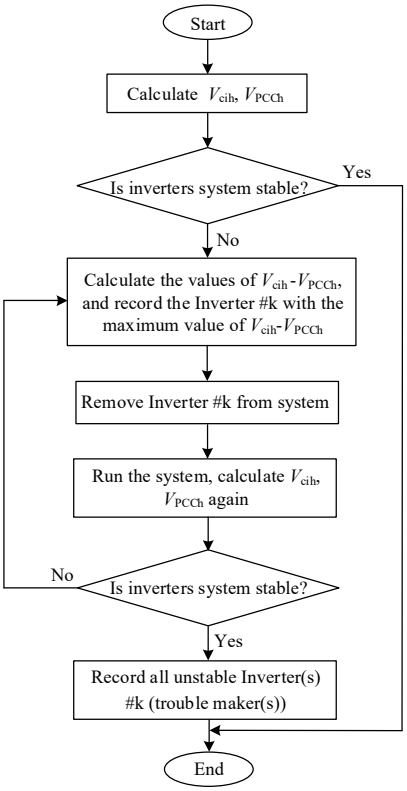

Fig. 6. The flowchart of the proposed auto-identification method.

TABLE I
SIMULATION AND EXPERIMENT PARAMETERS

Symbols	*Description*	*Value*
V_{g}	Grid voltage	110 V(RMS)
f, f_{s}	Grid, Switching and sampling frequency	50 Hz，10 kHz
L_1	Inverter side inductor	1.2 mH
C	Filter capacitor	6 uF
L_2	Grid side inductor	1.2 mH
L_{g}	Grid inductor	0.8 mH, 2 mH
U_{dc}	DC bus voltage	350 V

A. Simulation Verification

The main simulation parameters of the DC/AC inverters are listed in Table I. Fig. 7 shows the closed-loop pole-zero movement of T(s) with the control proportional gain of K_P in variation. It can be seen that the inverter is unstable, when K_P is 24 or 30.

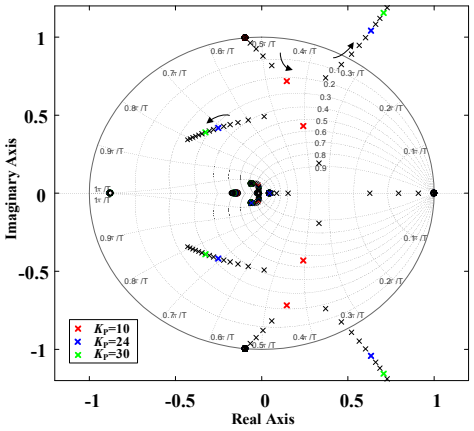

Fig.7. Closed-loop pole-zero movement of T(s) under $K_P$variation.

Two different operating cases were investigated:

Case I: Only one unstable inverter in the multi-paralleled inverters system (L_g=0.8 mH)

Case I shows how to identify the unstable inverter within a multi-paralleled inverters system interconnected with a stiff grid. The main control parameters are shown in Table II. The simulated PCC voltage and the total grid-injected currents of the entire inverters system is shown in Fig. 8 (a) and (b),

TABLE II
CONTROLLER PARAMETERS in CASE I

Inverter number	*The value of PR controller*		*Stability*
Inverter #1	K_{P1}	30	unstable
	K_{r1}	1000	
Inverter #2	K_{P2}	10	stable
	K_{r2}	1000	
Inverter #3	K_{P3}	10	stable
	K_{r3}	1000	
Inverter #4	K_{P4}	10	stable
	K_{r4}	1000	

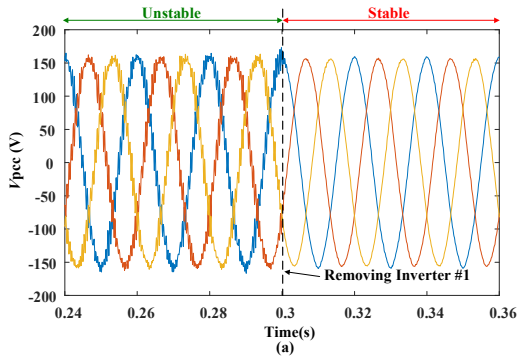

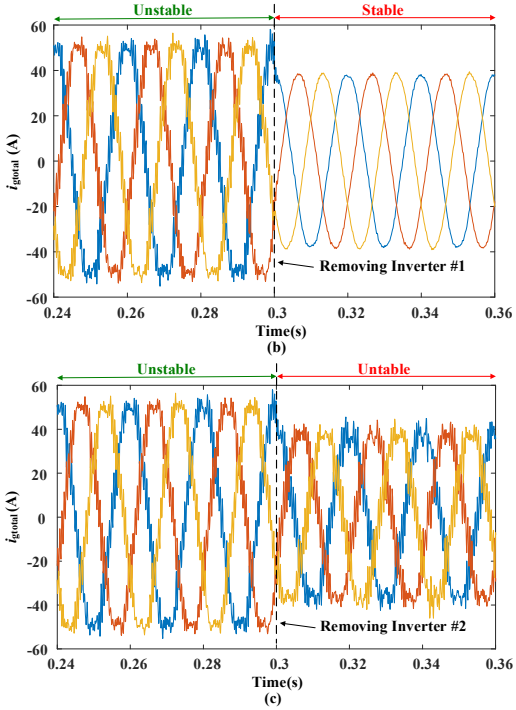

Fig.8. Simulation results in Case I: (a) waveform of the PCC voltage when disconnecting Inverter #1. (b) waveform of the total grid-injected current of the inverters system when disconnecting Inverter #1. (c) waveform of the total grid-injected current of the inverters system when disconnecting Inverter #2.

respectively. The filtered RMS values V_{c1h},V_{c2h}, V_{c3h},V_{c4h} and V_{PCCh} are shown in Fig. 9. Before the time instant of 0.3 s, it holds that V_{c1h} > 8.8 V, V_{c2h} > 8.8 V, V_{c3h} > 8.8 V, V_{c4h} > 8.8 V and V_{PCCh} > 8.8 V, indicating that the system is unstable. According to Fig.9, V_{c1h}-V_{PCCh} ≈ 80 V, V_{c2h}-V_{PCCh} ≈ -5 V, V_{c3h}-V_{PCCh} ≈ -5 V, V_{c4h}-V_{PCCh} ≈ -5 V. The Inverter #1 is disconnected from the multi-paralleled inverters system at 0.3 s and the remaining system continues to operate. Then, it holds that V_{c1h} < 8.8 V, V_{c2h}< 8.8 V, V_{c3h}< 8.8 V, V_{c4h}< 8.8 V and V_{PCCh} < 8.8 V. It is concluded that DC/AC Inverter #1 is in internal instability and it can be identified as a "trouble maker".

According to equation (9), T_m (with Inverter #1) or T_m' (without Inverter #1), the ratio of the output admittances of inverters to grid admittance, can be used to judge the stability of inverters system. If T_m or T_m' satisfies the Nyquist stability criteria, then the inverters system is stable, otherwise it is unstable. As shown in Fig. 10(a), the Nyquist curve of T_m and T_m' does not cross from the left side of (-1, j0). In Fig. 10(b), pole-zero plot of T_m (with Inverter #1) includes two right-half-plane poles and pole-zero plot of T_m' (without Inverter #1) has no poles in the right half plane. Because the number of turns of the Nyquist curve of T_m around the (-1, j0) point counterclockwise is equal to 0, the number of poles of T_m in the right half plane is equal to 2. It means that T_m does not meet the Nyquist stability criteria. Similarly, T_m' meets the Nyquist stability criteria. Therefore, when Inverter #1 is disconnected, the inverters system becomes stable again. Fig. 8 (a) and (b) also demonstrate that the multi-paralleled inverters system becomes stable again, when Inverter #1 is disconnected after the time instant of 0.3 s.

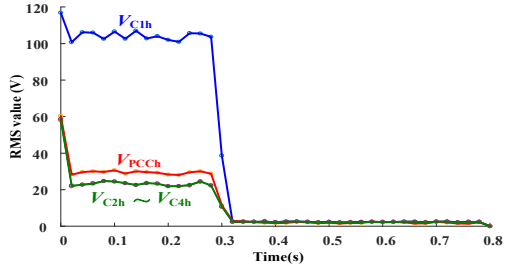

Fig.9. The RMS values of V_{c1h}, V_{c2h}, V_{c3h}, V_{c4h} and V_{PCCh} in Case I.

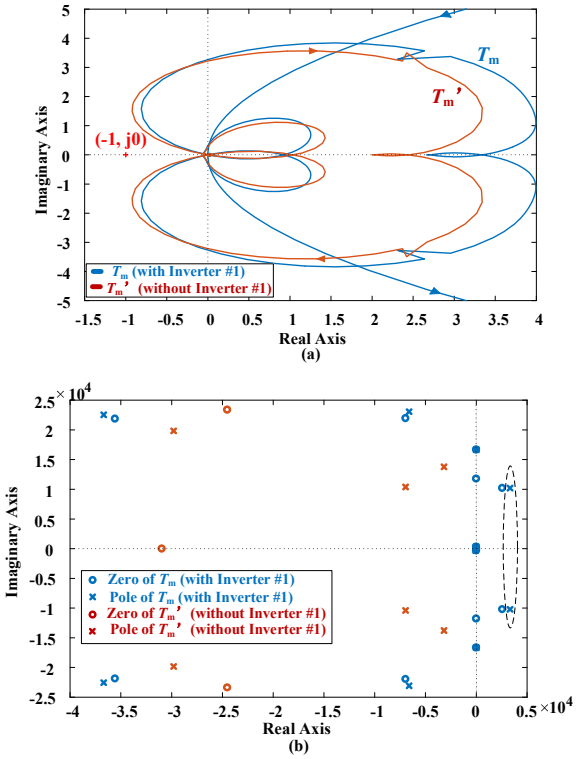

Fig. 10. （a）Nyquist plot of T_m and T_m' (T_m=(Y_{01}+Y_{02}+Y_{03}+Y_{04})/Y_g, T_m'=(Y_{02}+Y_{03}+Y_{04})/Y_g), (b) pole-zero plot of T_m and T_m'.

In contrast, as shown in Fig. 8(c), the multi-paralleled inverters system is still unstable when the operation of Inverter #2 is disabled after the time instant of 0.3 s.

Case II: Multi-unstable inverters in system (L_g=2mH)

TABLE III
CONTROLLER PARAMETERS in CASE II

Inverter number	*The value of PR controller*		*Stability*
Inverter #1	K_{P1}	30	unstable
	K_{r1}	1000	
Inverter #2	K_{P2}	24	unstable
	K_{r2}	1000	
Inverter #3	K_{P3}	10	stable
	K_{r3}	1000	
Inverter #4	K_{P4}	10	stable
	K_{r4}	1000	

Case II corresponds to an example where the proposed method is utilized to identify two unstable inverters within a multi-paralleled inverters system. The controller parameters in Case II are shown in Table III. Fig. 11 shows the simulated PCC voltage and the total grid-injected current of the inverters system. Fig. 12 shows the filtered RMS values of V_{c1h}, V_{c2h}, V_{c3h}, V_{c4h} and V_{PCCh}. Before the time instant of 0.3 s, the voltage of PCC and the total grid-injected current of the inverters system are oscillating. Meanwhile, Fig. 12 shows that V_{c1h} > 8.8 V, V_{c2h} > 8.8 V, V_{c3h} > 8.8 V, V_{c4h} > 8.8 V, and V_{PCCh} > 8.8 V, which indicates that the multi-paralleled inverters system is unstable. At the same time, V_{c1h}-V_{PCCh} ≈ 73 V, V_{c2h}-V_{PCCh} ≈ 67 V, V_{c3h}-V_{PCCh} ≈ 2 V, and V_{c4h}-V_{PCCh} ≈ 2V. Then, Inverter #1 with the maximum of V_{cih}-V_{PCCh} is disconnected from the inverters system at 0.3 s and only the remaining system continues to operate. After the time of 0.3 s V_{c2h} > 8V, V_{c3h} > 8V, V_{c4h} > 8V, V_{PCCh} > 8V, indicating that the remaining inverters system is still unstable. Fig. 11(a) and (b) also show that the remaining inverters system is unstable between 0.3 s and 0.4 s, due to V_{c2h}-V_{PCCh}≈ 61 V >0 V, V_{c3h}-V_{PCCh}≈ -13 V <0 V, V_{c4h}-V_{PCCh}≈ -13 V < 0 V. At 0.4 s, the Inverter #2 is disconnected and the remaining system turns back to stable, where from Fig. 12, the filters capacitors harmonic voltages and the PCC voltage become V_{c1h} < 8.8 V, V_{c2h} < 8.8 V, V_{c3h} < 8.8 V, V_{c4h} < 8.8 V, and V_{PCCh} < 8.8 V. Therefore, the Inverter #1 and #2 can be identified as “trouble makers”.

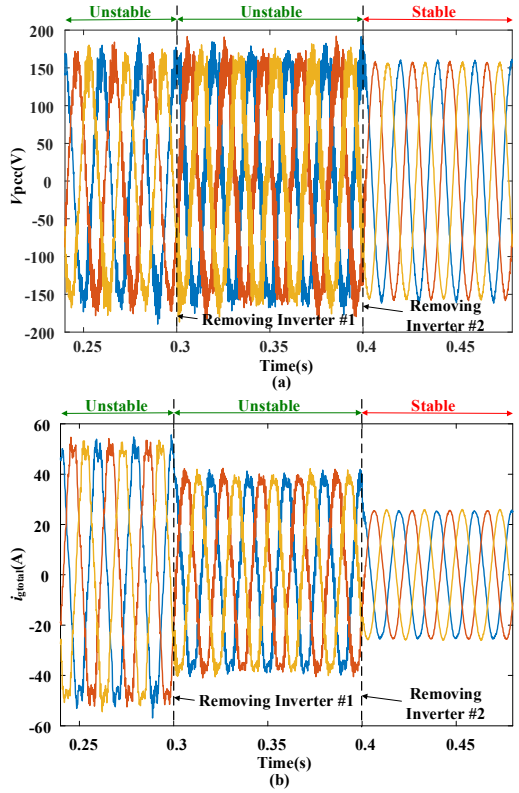

Fig.11. Simulation results in Case II: (a) waveform of the PCC voltage when disconnecting Inverter #1 and #2, respectively. (b) waveform of the total grid-injected current of the inverters system when disconnecting Inverter #1 and #2, respectively.

This article has been accepted for publication in a future issue of this journal, but has not been fully edited. Content may change prior to final publication. Citation information: DOI 10.1109/TIE.2021.3053881, IEEE Transactions on Industrial Electronics

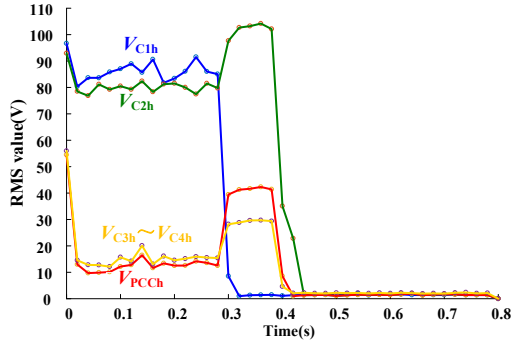

Fig.12. RMS values of V_{c1h}, V_{c2h}, V_{c3h}, V_{c4h} and V_{PCCh} in Case II.

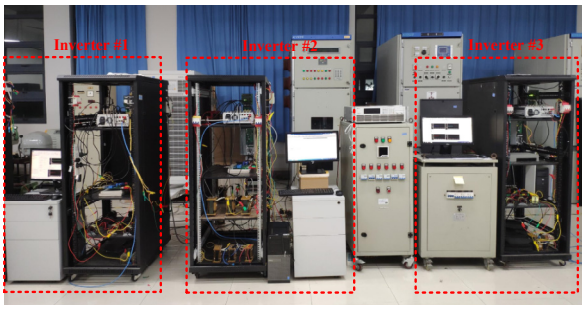

Fig. 13. Experimental Setup.

B. *Experimental Verification*

In order to further verify the effectiveness of the proposed method, three paralleled experimental DC/AC inverter prototypes of 110V/50Hz/2.4kW were implemented based on the dSPACE DS1202 control unit, the Danfoss-FC320 AC power drive and the Chroma 62150H-600S power supply. All the experimental waveforms were captured using a Yokogawa DL 1640 digital oscilloscope. The photo of the experimental setup is shown in Fig. 13.

During the experiment, the parameters (except for the reference currents) of the inverters in run are the same as those in the simulation.

Case I: Only one unstable inverter in the multi-paralleled inverters system (L_g=0.8 mH)

Fig. 14 shows the measured PCC voltage and total grid-injected currents of the entire inverters system.

As shown in Fig. 14, before T_1, the PCC voltage and the total grid-injected currents are unstable. Additionally, it holds that V_{c1h}- V_{PCCh}≈ 50 V, V_{c2h}- V_{PCCh}≈ -16 V, and V_{c2h}- V_{PCCh}≈ -17 V. Then, at the time instant of T_1, Inverter #1 is disconnected from the multi-paralleled inverters system and only the remaining system continues to operate, resulting in V_{c1h} < 8.8 V, V_{c2h} < 8.8 V, V_{c3h} < 8.8 V, and V_{PCCh} < 8.8 V. Therefore, it is indicated that Inverter #1 is under internal instability operating condition and can be identified as a "trouble maker".

Case II: Multi-unstable inverters in system (L_g=2mH)

Fig. 15 shows that the PCC voltage and the total grid-injected currents of the entire inverters system, where it can be seen that before the time instant of T_2, the system is unstable since V_{c1h}-V_{PCCh} ≈ 40 V, V_{c2h}-V_{PCCh} ≈ 35 V and V_{c3h}-V_{PCCh} ≈ 2 V.

Next, at time of T_2, Inverter #1 with the maximum of V_{cih} - V_{PCCh} is disconnected from the multi-paralleled inverters system and only the remaining system keeps operation. It can be seen that V_{c2h} > 8.8 V, V_{c3h} > 8.8 V and V_{PCCh} > 8.8 V, indicating that the remaining inverters system is still unstable. At time of T_3, Inverter #2 is removed further, where it can be seen that V_{c3h} < 8.8 V and V_{PCCh} < 8.8 V, showing that inverters system with only Inverter #3 becomes stable. Thus, Inverter #1 and #2 can be identified as "trouble makers".

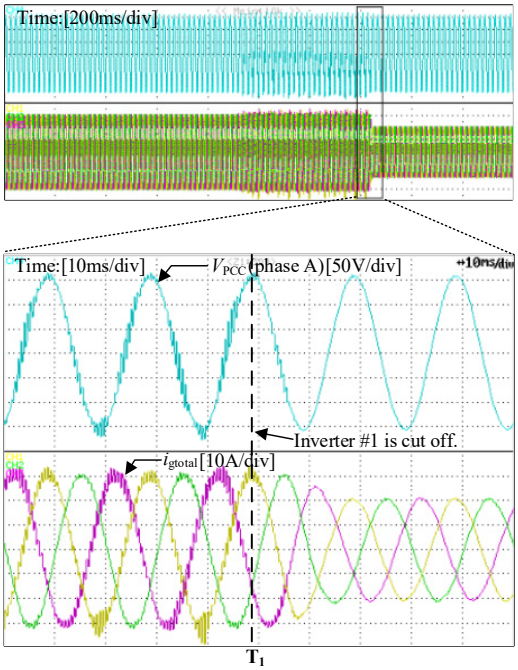

Fig.14. Experimental results of the system in Case I: waveforms of the PCC voltage of phase A and the total grid-injected current of the inverters system.

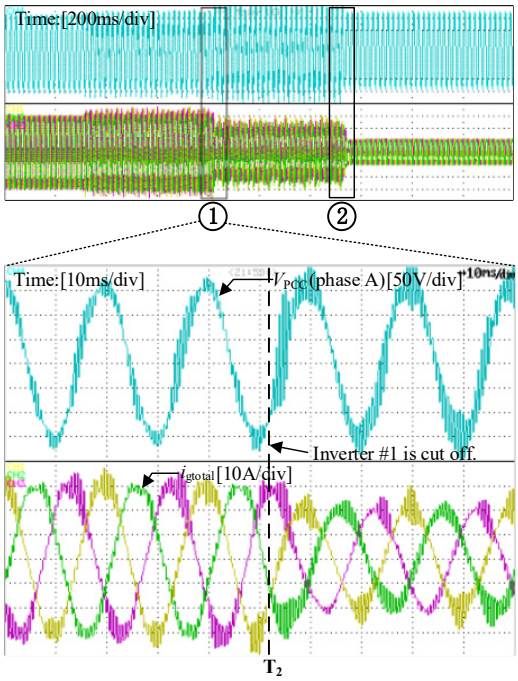

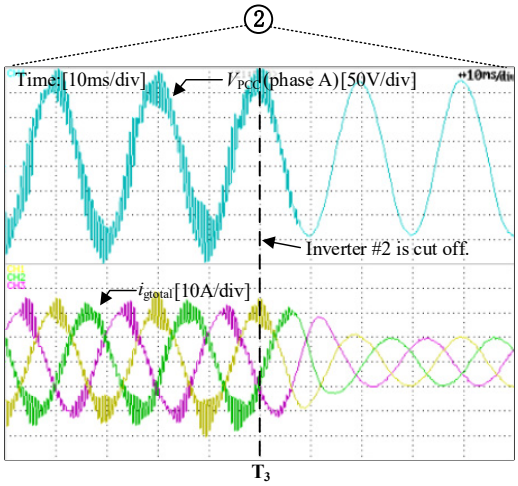

Fig.15. Experimental results of the system in Case II: waveforms of the PCC voltage of phase A and the total grid-injected current of the inverters system.

V. Conclusion

In this paper, a novel method to automatically identify the "trouble maker(s)" for internal instability in a multi-paralleled grid-connected inverters system has been proposed. The proposed diagnosis technique is based on the comparison between the RMS value of harmonic voltage at the PCC and the harmonic voltages across the filters capacitors. It comprises five steps to detect which individual inverter (or inverters) causes the instability of the overall multi-paralleled inverters system. The effectiveness of the proposed method has been verified by simulations and experiments exactly.

In future work it will be verified whether the proposed auto-identification method can also be used for the identification of the interactive instability that appears in a power -electronics-based AC Grid. Certainly, the auto-identification method of the instability that caused by the improperly designed PLL need be further explored.

References

[1] F. Blaabjerg, Z. Chen, S.B. Kjaer, "Power electronics as efficient interface in dispersed power generation systems," *IEEE Trans. Power Electron*., vol. 19, no. 5, pp. 1184-1194, Sept. 2004.

[2] W. Wu, Y. He and F. Blaabjerg, "An LLCL power filter for single-phase grid-tied inverter," *IEEE Trans. Power Electron*., vol. 27, no. 2, pp. 782-789, Feb. 2012.

[3] W. Wu, Y. Liu, Y. He, H. S. Chung, M. Liserre and F. Blaabjerg, "Damping methods for resonances caused by LCL-filter-based current-controlled grid-tied power inverters: An Overview,"*IEEE Trans. Ind. Electron.*, vol. 64, no. 9, pp. 7402-7413, Sept. 2017.

[4] D. Pan, X. Ruan, C. Bao, W. Li and X. Wang, "Capacitor-current-feedback active damping with reduced computation delay for improving robustness of LCL-type grid-connected Inverter," *IEEE Trans. Power Electron.*, vol. 29, no. 7, pp. 3414-3427, July 2014.

[5] J. Sun, "Impedance-based stability criterion for grid-connected inverters," *IEEE Trans. Power Electron*., vol. 26, no. 11, pp. 3075-3078, Nov. 2011.

[6] Y. Wang, X. Wang, F. Blaabjerg, and Z. Chen, "Harmonic instability assessment using state-space modeling and participation analysis in inverter-fed power systems," *IEEE Trans. Ind. Electron.*, vol. 64, no. 1,pp. 806–816, Jan. 2017.

[7] L. Jia, X. Ruan, W. Zhao, Z. Lin and X. Wang, "An adaptive active damper for improving the stability of grid-connected inverters under weak grid," *IEEE Trans. Power Electron.*, vol. 33, no. 11, pp. 9561-9574, Nov. 2018.

[8] Z. Zhang, W. Wu, Z. Shuai, X. Wang, A. Luo, H. S. Chung, and F. Blaabjerg, "Principle and robust impedance-based design of grid-tied inverter with LLCL-Filter under wide variation of grid-reactance," *IEEE Trans. Power Electron.*, vol. 34, no. 5, pp. 4362-4374, May 2019 .

[9] J. Agorreta, M. Borrega, J. Lopez, and L. Marroyo, "Modeling and control of N-paralleled grid-connected inverters with LCL filters coupled due to grid impedance in PV plants," *IEEE Trans. Power Electron.*, vol. 26, no. 3, pp. 770-1194, Mar. 2011.

[10] J. He, Y. Li, D. Bosnjak, "Investigation and active damping of multiple resonances in a parallel-inverter-based microgrid," *IEEE Trans. Power Electron.*, vol. 28, no. 1, pp. 234-246, Jan. 2013.

[11] H. Hu, Q. Shi, Z. He, J. He, and S. Gao, "Potential harmonic resonance impacts of PV inverter filters on distribution systems," *IEEE Trans. Sustain. Energy*, vol. 6, no. 1, pp. 151–161, Jan. 2015.

[12] C. Zhang, M. Molinas, A. Rygg and X. Cai, "Impedance-based analysis of interconnected power electronics systems: impedance network modeling and comparative studies of stability criteria," *IEEE Journal of Emerging and Selected Topics in Power Electron.*, vol. 8, no. 3, pp. 2520-2533, Sept. 2020.

[13] H. Bai, X. Wang and F. Blaabjerg, "Passivity enhancement in renewable energy source based power plant with paralleled grid-connected VSIs," *IEEE Trans. Ind. Appl.*, vol. 53, no. 4, pp. 3793-3802, July-Aug. 2017.

[14] X. Wang and F. Blaabjerg, "Harmonic stability in power electronic-based power systems: concept, modeling, and analysis," *IEEE Trans. Smart Grid.*, vol. 10, no. 3, pp. 2858-2870, May 2019.

[15] Y. Han *et al*., "Modeling and stability analysis of LCL-type grid-connected inverters: a comprehensive overview," *IEEE Access.*, vol. 7, pp. 114975-115001, 2019.

[16] M. Lu, X. Wang, P. C. Loh and F. Blaabjerg, "Resonance interaction of multi-parallel grid-connected inverters with LCL filter," *IEEE Trans. Power Electron.*, vol. 32, no. 2, pp. 894-899, Feb. 2017.

[17] M. Lu, Y. Yang, B. Johnson and F. Blaabjerg, "An interaction-admittance model for multi-inverter grid-connected systems," *IEEE Trans. Power Electron.*, vol. 34, no. 8, pp. 7542-7557, Aug. 2019.

[18] T. Chen, C. Lee and S. Y. R. Hui, "A general design procedure for multi-parallel modular grid-tied inverters system to prevent common and interactive instability," *IEEE Trans. Power Electron.*, vol. 34, no. 7, pp. 6025-6030, July 2019.

[19] X. Wang, F. Blaabjerg, M. Liserre, Z. Chen, J. He, and Y. Li, "An active damper for stabilizing power-electronics-based ac systems, "*IEEE Trans. Power Electron*., vol. 29, no. 7, pp. 3318–3329, Jul. 2014.

[20] Y. Guo, X. Lu, L. Chen, T. Zheng, J. Wang and S. Mei, "Functional-rotation-based active dampers in AC microgrids with multiple parallel interface inverters," *IEEE Trans. Ind. Appl.*, vol. 54, no. 5, pp. 5206-5215, Sept.-Oct. 2018.

[21] L. Yang, Y. Chen, A. Luo and K. Huai, "Stability enhancement for parallel grid-connected inverters by improved notch filter," *IEEE Access*, vol. 7, pp. 65667-65678, 2019.

[22] E. Ebrahimzadeh, F. Blaabjerg, X. Wang, and C. L. Bak,"Bus participation factor analysis for harmonic instability in power electronics-based power systems,"*IEEE Trans. Power Electron.*, vol. 33, no. 12, pp. 10341–10351, Dec. 2018.

[23] X. Wang, F. Blaabjerg and W. Wu, "Modeling and analysis of harmonic stability in ac power-electronics-based power system," *IEEE Trans. Power Electron.*, vol. 29, no. 12, pp. 6421-6432, Dec. 2014.

[24] W. Cao, S. Wang, K. Liu, H. Kang and J. Zhao, "Responsibility identification for harmonic oscillation issues in the parallel grid-connected inverters system," *IEEE Access*., vol. 7, pp. 171061-171072, 2019.

[25] B. Wen, D. Dong, D. Boroyevich, R. Burgos, P. Mattavelli and Z. Shen, "Impedance-based analysis of grid-synchronization stability for three-phase paralleled converters," *IEEE Trans. Power Electron.*, vol. 31, no. 1, pp. 26-38, Jan. 2016.

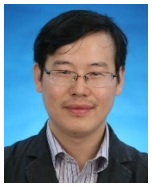

Weimin Wu (M'16) received Ph.D. degrees in Electrical Engineering from the College of Electrical Engineering, Zhejiang University, Hangzhou, China, in 2005.

He worked as a research engineer in the Delta Power Electronic Center (DPEC), Shanghai, from July, 2005 to June, 2006. Since July, 2006, he has been a Faculty Member at Shanghai Maritime University, where he is currently a Full Professor in Department of Electrical Engineering. He was a Visiting Professor in the Center for Power Electronics Systems (CPES), Virginia Polytechnic Institute and State University, Blacksburg, USA, from Sept. 2008 to March. 2009. From Nov. 2011 to Jan. 2014, he was also a visiting professor in the Department of Energy Technology, Aalborg University, Demark, working at the Center of Reliable Power Electronics (CORPE). He has coauthored over 100 papers and holds eight patents. His areas of interests include power converters for renewable energy systems, power quality, smart grid, and energy storage technology. Dr. Wu serves as an Associate Editor for the IEEE TRANSACTIONS ON INDUSTRY ELECTRONICS.

Zhijun Zhao was born in Henan, China, in 1994. He received the B.S. degree in electrical engineering from Shanghai Maritime University, Shanghai, China, in 2018, where he is currently pursuing the M.S. degree in electrical engineering. His current research interests include modeling and stability analysis of VSC-based energy conversion systems.

Eftichis Koutroulis (M'10–SM'15) was born in Chania, Greece, in 1973. He received the Diploma, M.Sc., and Ph.D. degrees in electronic and computer engineering from the Technical University of Crete, in 1996, 1999, and 2002, respectively.

In September 2002 he has served at the Department of Electronic and Computer Engineering, Technical University of Crete. He worked as a Visiting Researcher at the Department of Energy Technology, Aalborg University, Aalborg, Denmark. Since January 2012, he has been an Assistant Professor with the Department of Electronic and Computer Engineering, Technical University of Crete. His research interests include the design of power converters and microelectronic energy management systems for renewable energy sources applications and the design optimization of photovoltaic power plants. Since April 2011, he has been serving as a member of the Editorial Board of the Renewable Energy Journal.

Henry Shu-Hung Chung (M'95-SM'03-F'16) received the B.Eng. and Ph.D. degrees in electrical engineering from the Hong Kong Polytechnic University, Kowloon, Hong Kong, in 1991 and 1994, respectively.

Since 1995, he has been with the City University of Hong Kong, Kowloon, where he is currently a Chair Professor in the Department of Electrical Engineering and the Director of the Center for Smart Energy Conversion and Utilization Research. His current research interests include renewable energy conversion technologies, lighting technologies, smart grid technologies, and computational intelligence for power electronic systems. He has edited one book, authored eight research book chapters, and over 460 technical papers including 200 refereed journal papers in his research areas, and holds 50 patents.

Dr. Chung was the Chair of the Technical Committee of the High-Performance and Emerging Technologies, IEEE Power Electronics Society in 2010-2014. He is currently Associate Editor of the IEEE Transactions on Power Electronics and the IEEE Journal of Emerging and Selected Topics in Power Electronics. He was Editor-in-Chief of the IEEE Power Electronics Letters 2014-2018. He has received numerous industrial awards for his invented energy saving technologies.

Frede Blaabjerg (S'86–M'88–SM'97–F'03) was with ABB-Scandia, Randers, Denmark, from 1987 to 1988. From 1988 to 1992, he got the PhD degree in Electrical Engineering at Aalborg University in 1995. He became an Assistant Professor in 1992, an Associate Professor in 1996, and a Full Professor of power electronics and drives in 1998. From 2017 he became a Villum Investigator. He is honoris causa at University Politehnica Timisoara (UPT), Romania and Tallinn Technical University (TTU) in Estonia.

His current research interests include power electronics and its applications such as in wind turbines, PV systems, reliability, harmonics and adjustable speed drives. He has published more than 600 journal papers in the fields of power electronics and its applications. He is the co-author of four monographs and editor of ten books in power electronics and its applications.

He has received 32 IEEE Prize Paper Awards, the IEEE PELS Distinguished Service Award in 2009, the EPE-PEMC Council Award in 2010, the IEEE William E. Newell Power Electronics Award 2014, the Villum Kann Rasmussen Research Award 2014, the Global Energy Prize in 2019 and the 2020 IEEE Edison Medal. He was the Editor-in-Chief of the IEEE TRANSACTIONS ON POWER ELECTRONICS from 2006 to 2012. He has been distinguished Lecturer for the IEEE Power Electronics Society from 2005 to 2007 and for the IEEE Industry Applications Society from 2010 to 2011 as well as 2017 to 2018. In 2019-2020 he serves a President of IEEE Power Electronics Society. He is Vice-President of the Danish Academy of Technical Sciences too.

He is nominated in 2014-2019 by Thomson Reuters to be between the most 250 cited researchers in Engineering in the world.